

Metastable helium molecules as tracers in superfluid liquid ^4He

W. Guo, J.D. Wright, S.B. Cahn, J.A. Nikkel, and D.N. McKinsey
Physics department, Yale University, New Haven, CT 06515

(Dated: February 12, 2022)

Metastable helium molecules generated in a discharge near a sharp tungsten tip operated in either pulsed mode or continuous field-emission mode in superfluid liquid ^4He are imaged using a laser-induced-fluorescence technique. By pulsing the tip, a small cloud of He_2^* molecules is produced. At 2.0 K, the molecules in the liquid follow the motion of the normal fluid. We can determine the normal-fluid velocity in a heat-induced counterflow by tracing the position of a single molecule cloud. As we run the tip in continuous field-emission mode, a normal-fluid jet from the tip is generated and molecules are entrained in the jet. A focused 910 nm pump laser pulse is used to drive a small group of molecules to the vibrational $a(1)$ state. Subsequent imaging of the tagged $a(1)$ molecules with an expanded 925 nm probe laser pulse allows us to measure the velocity of the normal fluid. The techniques we developed demonstrate for the first time the ability to trace the normal-fluid component in superfluid helium using angstrom-sized particles.

PACS numbers: 47.27.-i, 29.40.Gx, 67.25.dk, 67.25.D-

Visualizing the flow of superfluid ^4He has long been of interest to the scientific community [1, 2]. Recently, particle image velocimetry with polymer micro-spheres and hydrogen isotopes has been used to study liquid helium flows [3, 4] and solid hydrogen tracers have been used to visualize the quantized vortices [5, 6]. However, the dynamics of micron-sized tracers in the presence of vortices are complex [3]. Kivotides [7] analyzed the results of Zhang and Van Sciver [3] and concluded that one must account for particle-vortex interactions [8] in order to extract an accurate measurement of the local normal-fluid velocity from experimental data obtained using micron-sized tracer particles. Furthermore, if the vortex-line density is too high then the possibility to use micron-sized particles to measure the normal-fluid velocity is lost. On the other hand, it has been shown that metastable He_2^* triplet molecules can be imaged using a laser-induced-fluorescence technique [9, 10]. The He_2^* molecules are much smaller in size (7 Å radius [11]) and should follow the motion of the normal fluid without being affected by vortices at temperatures above 1 K [12]. Although so far the sensitivity in imaging the molecules is not high enough to track the motions of individual molecules, useful studies can still be performed by tracking a group of molecules. [13] In this Letter we shall show in two demonstration experiments the methods we developed in tracing the true normal-fluid flow. In the first demonstration experiment, a cloud of He_2^* molecules was used as a single tracer. In the second experiment, a small group of He_2^* molecules was tagged and imaged using their internal vibrational levels.

Both experiments were conducted at 2.0 K. A sharp tungsten tip, made via a standard chemical etching technique [14], was used to produce the He_2^* molecules in liquid helium. It is known that He_2^* molecules in both spin singlet and triplet states are produced near the tip apex when a negative voltage with amplitude higher than the field-emission threshold is applied to the tip [15, 16].

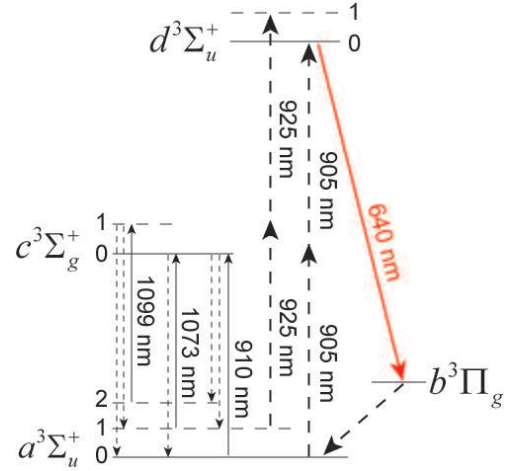


FIG. 1: Schematic diagram showing the cycling transitions for imaging the He_2^* triplet molecules.

The singlet molecules radiatively decay in a few nanoseconds [17], while the triplet molecules are metastable with a radiative lifetime of about 13 s in liquid ^4He [18]. The widths of the He_2^* molecule absorption spectral lines in liquid helium (120 cm^{-1} [19]) are considerably larger than the spacings of the rotational levels ($\sim 7 \text{ cm}^{-1}$ [20]). A single pulsed laser at 905 nm is able to drive triplet molecules out of the $a^3\Sigma_u^+$ state to produce fluorescence through a cycling transition (see Fig. 1) [10]. However, the vibrational levels are separated by about 1500 cm^{-1} [20], and the vibrational-relaxation time is on the order of 1 s [13]. Therefore, molecules falling to excited vibrational levels of the $a^3\Sigma_u^+$ state are trapped in off-resonant levels. Continuous fiber lasers at 1073 nm and 1099 nm were used to repump the molecules from the $a(1)$ to the $c(0)$ states and from the $a(2)$ to the $c(1)$ states respectively. Molecules in the c states have a chance to decay back to the $a(0)$ state and can be used again.

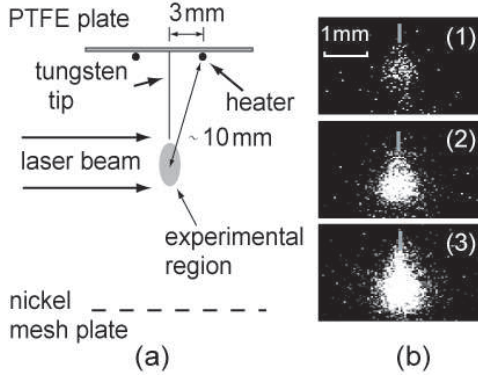


FIG. 2: (a) Schematic diagram showing the setup for the molecule cloud experiment. (b) Fluorescence images for He_2^* molecule clouds created with (1) 10 ms, (2) 30 ms and (3) 90 ms pulse on the tip, respectively. The grey bars indicate the tip. The images are a sum of 50 camera exposures.

In the first experiment, the tungsten tip was mounted at the center of a polytetrafluoroethene (PTFE) plate (see Fig. 2 (a)). The PTFE plate had a diameter of 21 mm and a thickness of 1 mm. To make a heater, four $100\ \Omega$ metal-film resistors were attached to the PTFE plate symmetrically around the tip. A nickel mesh plate was placed 3 cm away from the PTFE plate and was grounded. The whole device was held at the center of a helium cell with total volume of about $250\ \text{cm}^3$. The intensities of the fiber lasers at 1073 nm and 1099 nm were chosen to be $3\ \text{W}/\text{cm}^2$ and $1.5\ \text{W}/\text{cm}^2$ respectively. The intensity of the pulsed laser at 905 nm was $500\ \mu\text{J}/\text{cm}^2$ per pulse, and the repetition rate was 500 Hz. To create a small cloud of He_2^* molecules, a $-400\ \text{V}$ pulse is delivered to the tungsten tip through a $0.1\ \mu\text{F}$ capacitor in addition to a constant voltage of $-450\ \text{V}$. Electrons are emitted from the tungsten tip when the total voltage crosses the field-emission threshold (around $-550\ \text{V}$) during the pulse. A small cloud of molecules is created near the apex of the tip as the electrons move a short distance, lose their energy, and form bubbles in the liquid [21]. At 2.0 K, a He_2^* molecule diffuses less than 1 mm during its lifetime [9]. Thus the molecule cloud stays together and serves as a single tracer. The size of the molecule cloud is of the order of 1 mm but becomes larger for longer pulse durations. Typical images of a molecule cloud generated with 10 ms, 30 ms and 90 ms wide pulses are shown in Fig. 2 (b). These images were taken with an intensified CCD camera just after application of the voltage pulse to the tip. The camera was synchronized to each laser pulse and exposed for $6\ \mu\text{s}$ so as to minimize the dark current.

With the heater off, the molecule cloud was observed to drift towards the nickel mesh plate. The drift speed depended on the length of the voltage pulse on the tip. This effect results from a transient pulling force on the normal fluid created by the moving electron bubbles [16]. In or-

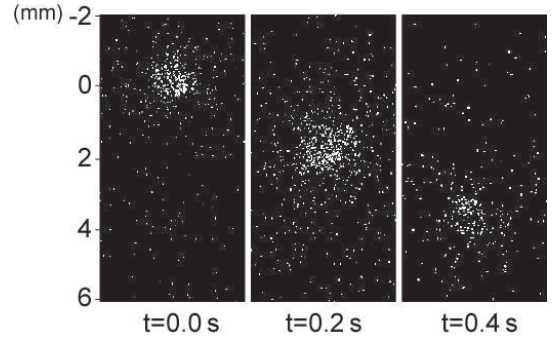


FIG. 3: The motion of a molecule cloud with 15V on the heater. The images were taken at 0 s, 0.2 s and 0.4 s respectively after the cloud was created. The duration of the pulse on the tungsten tip was 5 ms. The images are a sum of 25 camera exposures.

der to reduce this effect but also create enough molecules for good image quality, a voltage pulse of 5 ms duration was used. The corresponding drift velocity of the molecule cloud was about $1.8\ \text{mm}/\text{s}$.

As we turned on the heater, a thermal counterflow was set up in the liquid. The normal fluid flowed away from the heater with a speed v_n given in theory as [22]

$$v_n = \frac{Q/A}{\rho S T}. \quad (1)$$

where Q and A are the heat power and cross-section for heat transfer; ρ , S and T are the helium density, entropy and temperature respectively. Near the tip apex, the normal-fluid velocity was parallel to the tip due to the geometry. A typical set of images showing the motion of a molecule cloud with 15 V on the heater is shown in Fig. 3. The heater was turned on a few seconds before the molecule cloud was generated so as to set up a steady flow of the normal fluid. The three images in Fig. 3 were taken at 0 s, 0.2 s and 0.4 s respectively after the cloud was created. The number of camera exposures for each image was chosen to be 25 in order to obtain a good signal-to-noise ratio yet reduce image smearing. To determine the flow velocity, we fit the image of each molecule cloud with a Gaussian function. The maximum of the Gaussian gave the center position for each cloud. For a given drift time, several images were taken and an averaged center position was determined. In Fig. 4 (a), we show the data obtained for the averaged vertical position of each molecule cloud as a function of its drift time. The solid lines in Fig. 4 (a) are linear fits to the data. The slopes of those solid lines give the corresponding flow velocities. In Fig. 4 (b), we plot the normal-fluid velocity obtained as a function of the heat power. For low heat power, the normal fluid was believed to be in the laminar flow regime. Heat was transferred to all directions below the PTFE plate. The cross-section for heat transfer in this case was estimated to be about $6.2\ \text{cm}^2$.

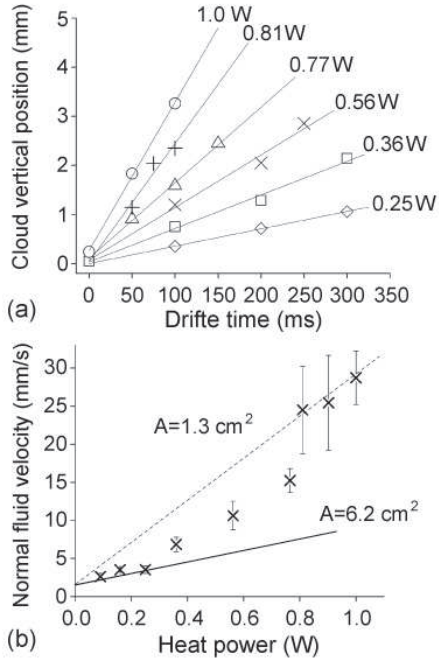


FIG. 4: (a) The average vertical positions of a molecule cloud as a function of its drift time for different heat powers. (b) The obtained normal-fluid velocity as a function of the heat power. The solid line and the dashed line are the theoretical curves as discussed in the text.

The solid line in Fig. 4 (b) shows the theoretical curve based on Eq. (1). However, as one can see, the measured data starts to deviate from the theoretical curve when the heat power is above roughly 0.25 W. If we take the typical length scale for the flow to be 1 cm, then the measured fluid velocity (3 mm/s) gives a Reynolds number as high as 3000. It is likely that the normal-fluid flow started to become turbulent and caused a change in heat transfer pattern. When the heat power is higher than 0.8 W, the turbulent flow in the normal-fluid may be fully developed and the dispersion of the measured flow velocity is large. The dashed line in Fig. 4 (b) shows the theoretical curve assuming an effective heat transfer cross-section of 1.3 cm^2 . A smaller effective heat transfer cross-section means most of the heat is transferred along the tip direction, for which no good explanation has yet been found.

In the second experiment, we created a continuous molecular beam and selectively imaged a small group of molecules which were tagged using the first excited vibrational level of the $a^3\Sigma_u^+$ electronic state. To create the molecular beam, we ran the tungsten tip in a continuous mode by applying a DC voltage higher than the field-emission threshold. The field-emission current was controlled to be less than 2.5 nA to keep the electric heating negligible. The emitted electrons moved from the tip to the nickel mesh plate leading to a continu-

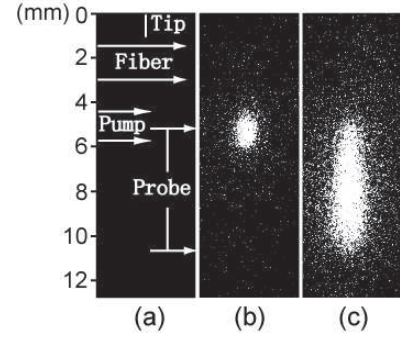


FIG. 5: (a) Schematic diagram showing the lasers used in the molecule tagging experiment. (b) and (c) show the molecule fluorescence images taken with pump laser alone and probe laser alone, respectively. Both the pump and the probe lasers were tuned to 905 nm in order to show the beam sizes and positions of the lasers.

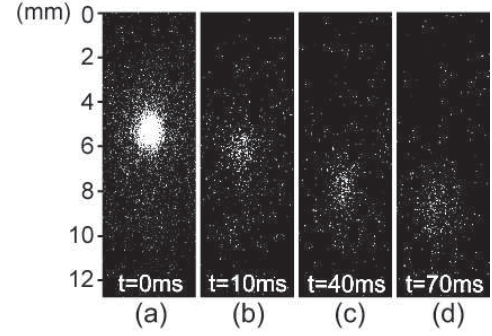


FIG. 6: Fluorescence images showing the positions of a small group of $a(1)$ molecules at different delay time after they were created. The delay time between the pump and probe laser pulses is (a) 0 ms, (b) 10 ms, (c) 40 ms and (d) 70 ms. The DC voltage on the tungsten tip was 805V.

ous pulling force on the normal fluid. A normal fluid jet was formed from the tip to the nickel mesh plate carrying the He_2^* molecules along [16]. Molecules created by field-emission initially occupy the $a(0)$, $a(1)$, and $a(2)$ excited states. To prepare a pure population of $a(0)$ -state molecules for tagging and eliminate background signal for selective imaging, the 1073 nm and 1099 nm fiber lasers were used to illuminate a small volume near the tip and drive molecules from the $a(1)$ and $a(2)$ excited vibrational levels into the $a(0)$ state. Then, as shown in Fig. 5, a focused pump laser at 910 nm was used to tag He_2^* molecules by driving population from the $a(0)$ to the $c(0)$ state and relying on redistribution of the $c(0)$ population into the long-lived $a(1)$ state (see Fig. 1) via non-radiative transitions which naturally occur in a few nanoseconds [13]. An expanded probe laser at 925 nm was then used to selectively image the tagged molecules by driving the $a(1)$ population into the d state and inducing 640 nm fluorescence via $d \rightarrow b$ radiative decay.

In Fig. 6, we show images for a group of tagged $a(1)$

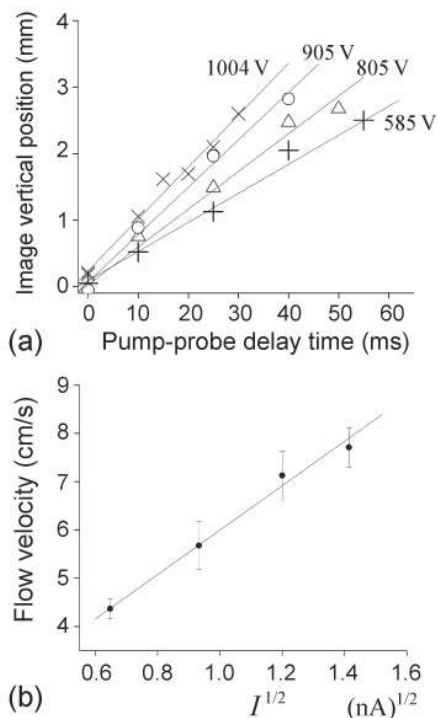


FIG. 7: (a) The vertical position of the $a(1)$ molecule cloud as a function of the pump-probe delay time at several different DC voltages on the tip. (b) Obtained normal-fluid velocity as a function of the square root of the current measured on the nickel mesh plate.

molecules taken at pump-probe delay time of 0 ms, 10 ms, 40 ms and 70 ms respectively with 805 V on the tip. Both the pump laser and probe laser had a pulse energy of 5 mJ and repetition rate of 10 Hz. At each fixed pump-probe delay time, the camera was exposed ten times to obtain a single image with a good signal-to-noise ratio. The bright image obtained with zero delay time resulted from a two-photon transition induced by the pump laser alone at 910 nm [13]. We also tested another way of producing $a(1)$ molecules by tuning the pump laser to 805 nm to drive the $a(0)$ molecules to the $a(1)$ state through the $c(1)$ state. The signal strength obtained this way is comparable to the one with the pump laser tuned to 910 nm. In Fig. 7 (a), we show the vertical position of the tagged $a(1)$ molecules as a function of the pump-probe delay time. The solid curves in Fig. 7 (a) are the linear fits to the data, and their slopes give the corresponding flow velocity. The total driving force on the normal fluid exerted by the moving electron bubbles is proportional to the electric current I [16]. In steady state the driving force on the jet is balanced by the drag force coming from the neighboring normal fluid. If we take the typical length for the jet flow to be 1 mm (the width of the jet), the Reynolds number is estimated to be $\sim 5 \times 10^3$. The flow should be in the turbulent regime, hence a drag force proportional to the square of the flow velocity is

expected [22]. In Fig. 7 (b), the obtained flow velocity is plotted as a function of $I^{1/2}$. A linear dependence is observed.

A similar result was discussed in Mehrotra's paper [16]. In their experiments, a pair of mesh grids were placed right in front of the tip to block the electric current while another pair was placed some distance away to detect the He_2^* molecules. They pulsed their tip on for about a second and then measured the time of flight of the neutral molecules to determine the average drift speed. Compared to their method, our technique has many advantages. For example, we can measure the flow velocity in the steady state with the tip running all the time and map out the velocity field along the jet.

In conclusion, we have developed practical techniques to trace the normal-fluid component in superfluid ^4He using metastable He_2^* molecules. Interesting hydrodynamic phenomena in the normal fluid were observed in the two demonstration experiments using these techniques. The ability to track the true normal-fluid flow provides direct understanding of the hydrodynamics of the normal-fluid component in superfluid ^4He , which will in turn feed into a better understanding of this unique two fluid system.

-
- [1] D.Y. Chung and P.R. Crichtlow, Phys. Rev. Lett. **14**, 892C894 (1965).
 - [2] M. Murakami and N. Ichikawa, Cryogenics **29**, 438C443 (1989).
 - [3] T. Zhang and S.W. Van Sciver, J. Low Temp. Phys. **138**, 865 (2005).
 - [4] T. Zhang and S.W. Van Sciver, Nat. Phys. **1**, 36 (2005).
 - [5] G.P. Bewley, *et al.*, Nature **441**, 588 (2006).
 - [6] M.S. Paoletti, *et al.*, Phys. Rev. Lett. **101**, 154501 (2008).
 - [7] D. Kivotides, Phys. Rev. **B78**, 224501 (2008).
 - [8] D. Kivotides, *et al.*, Phys. Rev. **B77**, 014527 (2008).
 - [9] D.N. McKinsey, *et al.*, Phys. Rev. Lett. **95**, 111101 (2005).
 - [10] W.G. Rellergert, *et al.*, Phys. Rev. Lett. **100**, 025301 (2008).
 - [11] A.V. Benderskii, *et al.*, J. Chem. Phys. **117**, 1201 (2002).
 - [12] W.F. Vinen, in *Low Temperature Physics*, AIP Conf. Proc. No. **850** (AIP, New York, 2006), p. 169.
 - [13] W.G. Rellergert, Ph.D. thesis, Yale University, 2008.
 - [14] A. Golov and H. Ishimoto, J. Low Temp. Phys. **113**, 957 (1998).
 - [15] P.V.E. McClintock, *et al.*, Cryogenics **13**, 556 (1973).
 - [16] R. Mehrotra, *et al.*, J. Low Temp. Phys. **36**, 47 (1979).
 - [17] C.F. Chabalowski *et al.*, J. Chem. Phys. **90**, 2504 (1989).
 - [18] D.N. McKinsey, *et al.*, Phys. Rev. **A59**, 200 (1999).
 - [19] J.C. Hill, *et al.*, Phys. Rev. Lett. **26**, 1213 (1971).
 - [20] G. Herzberg, *Molecular Spectra And Molecular Structure Vol. I-Spectra Of Diatomic Molecules* (Krieger, Malabar, FL, 1950).
 - [21] J.S. Adams, Ph.D. thesis, Brown University, 2001.
 - [22] L.D. Landau and E.M. Lifshitz, *Fluid Mechanics*, (New York, 1987) 2nd edition.